Push the Envelope

Bumman Kim, Jungjoon Kim, Dongsu Kim, Junghwan Son, Yunsung Cho, Jooseung Kim, and Byungjoon Park

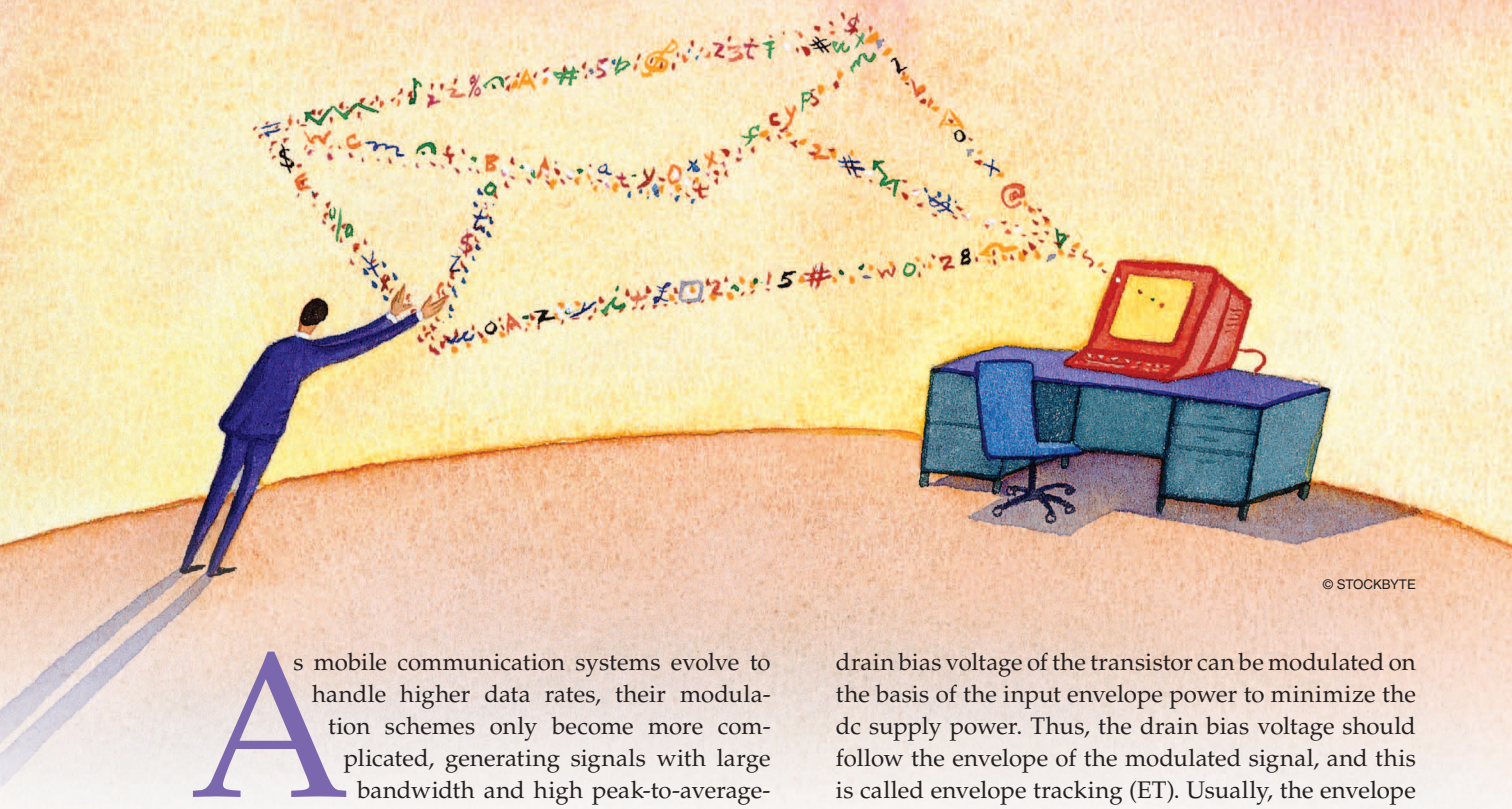

As mobile communication systems evolve to handle higher data rates, their modulation schemes only become more complicated, generating signals with large bandwidth and high peak-to-average-power ratio (PAPR). To amplify such signals with high efficiency, the power amplifier (PA) should have high efficiency not only at the peak power level but also at low power, especially over the maximum power generation region. To realize these PA characteristics, the drain bias voltage of the transistor can be modulated on the basis of the input envelope power to minimize the dc supply power. Thus, the drain bias voltage should follow the envelope of the modulated signal, and this is called envelope tracking (ET). Usually, the envelope is shaped to realize the optimum performance from the ET PA. The PA is biased close to class B, and the dc current is automatically adjusted to the power level. The resulting PA has high efficiency for all power levels, comparable to the maximum efficiency of the PA

Bumman Kim (bmkim@postech.ac.kr), Jungjoon Kim, Dongsu Kim, Junghwan Son, Yunsung Cho, Jooseung Kim, and Byungjoon Park are with the Department of Electrical Engineering and Division of IT Convergence Engineering, Pohang University of Science and Technology, San 31, Hyoja-dong, Nam-gu, Gyeungbuk 790-784, Republic of Korea.

Digital Object Identifier 10.1109/MMM.2013.2240851
Date of publication: 2 April 2013

at high power. In practice, the efficiency is degraded somewhat at low voltage because of the knee effect, lower transconductance, and mismatch effect for different drain bias voltages.

To supply the envelope signal to the drain for bias, the envelope signal should be amplified to a suitable level. The envelope signal has a bandwidth a few times larger than that of the modulated signal, and it is not an easy task to efficiently amplify a signal whose bandwidth is on the order of several tens of megahertz. Several supply modulators are available to amplify the signal, but, here, we introduce a hybrid switching amplifier (HSA), which is the most popular architecture.

The ET technique is ideal for multimode (MM)/multiband (MB) PAs: it simplifies broadbanding because the MM can be handled by the supply modulator and the PA's bandwidth then just needs to cover the RF band without any other restrictions. The supply modulator may be an ideal power management IC for PAs because the modulator powers the PA, and the performance of the PA can be optimized by implementing ET with the modulator. The ET technique is a powerful tool for PAs for both base stations and handsets. These advanced concepts of the ET technology are discussed in this article.

Basic Operation Principle

ET is employed to maintain high efficiency from the peak power level down to low power. In ET, the drain supply voltage is adjusted suitably for high efficiency at the given input power level. That is, for a modulated RF input signal, the supply voltage should follow the envelope signal. An envelope elimination and restoration (EER) technique was proposed for this purpose in 1952 by Kahn [1], but it has several problems, and ET is more popular nowadays. We will describe the differences between them. For proper ET, the envelope signal is not directly applied to the PA but is suitably reshaped to obtain the desired performance. The shaping methods will also be introduced.

Comparison Among Conventional PA, ET, and EER

The modulated signals in current wireless communication systems have a high PAPR, and conventional linear PAs operate at very low efficiency; thus, large power consumption is inevitable. To solve this problem, ET and EER techniques are employed by many researchers [1]–[21]. As shown in Figure 1, both techniques have similar circuit structures and operation principles. ET involves a supply modulator and a PA with a modulated RF input signal. In contrast, EER requires a supply modulator and a switching PA with a constant-envelope RF signal containing only the phase information. By modulating the supply voltage of the PA according to the output power level, the internal power consumption is minimized at all power levels and the efficiency for amplification of a modulated signal is improved. Although ET is very similar to EER, their characteristics are quite different owing to the input RF signals. In the case of the EER, the input is a constant-envelope phase-modulated RF signal and it uses a saturated switching PA. The constant-envelope phase-modulated RF signal has a very wide bandwidth, approximately ten times wider than that of the modulated signal. Thus, the Cordic, which generates the phase-modulated signal from the I and Q signals, should have a similarly wide bandwidth. Regardless of the output power level, because of the saturated operation of the switching PA and the constant-envelope phase-modulated RF input signal, the EER system has very low gain in low-power regions with low power-added efficiency (PAE). It also has a severe power leak problem at low power. Besides, the output power is proportional to the drain voltage and is highly sensitive to the supply voltage. Therefore, its linearity is directly related to the supply voltage linearity, which is rather poor. The synchronization between the constant-envelope phase-modulated RF signal and the modulated supply voltage should be very accurate. Otherwise, the signal can be distorted. However, the ET PA employs a modulated RF input signal and can use the same lin-

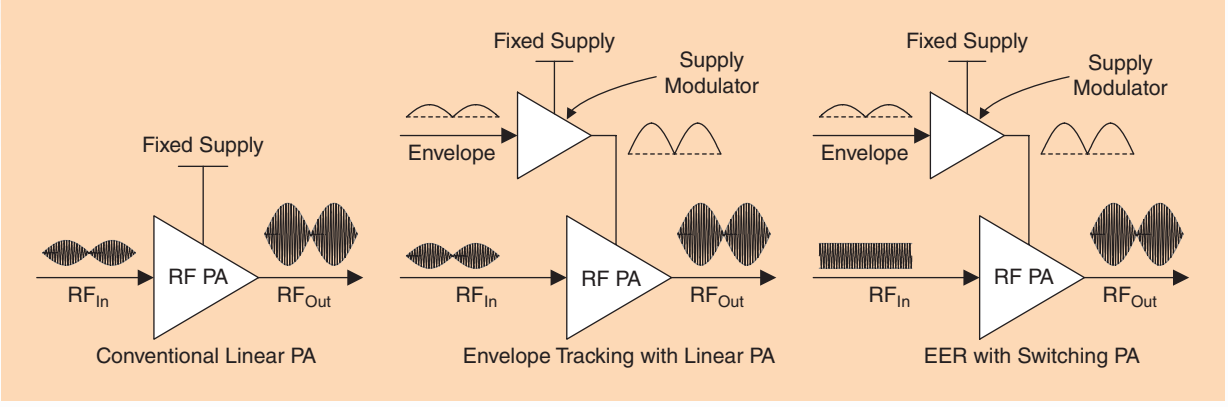

Figure 1. *Block diagrams of conventional linear PA, envelope tracking PA, and EER.*

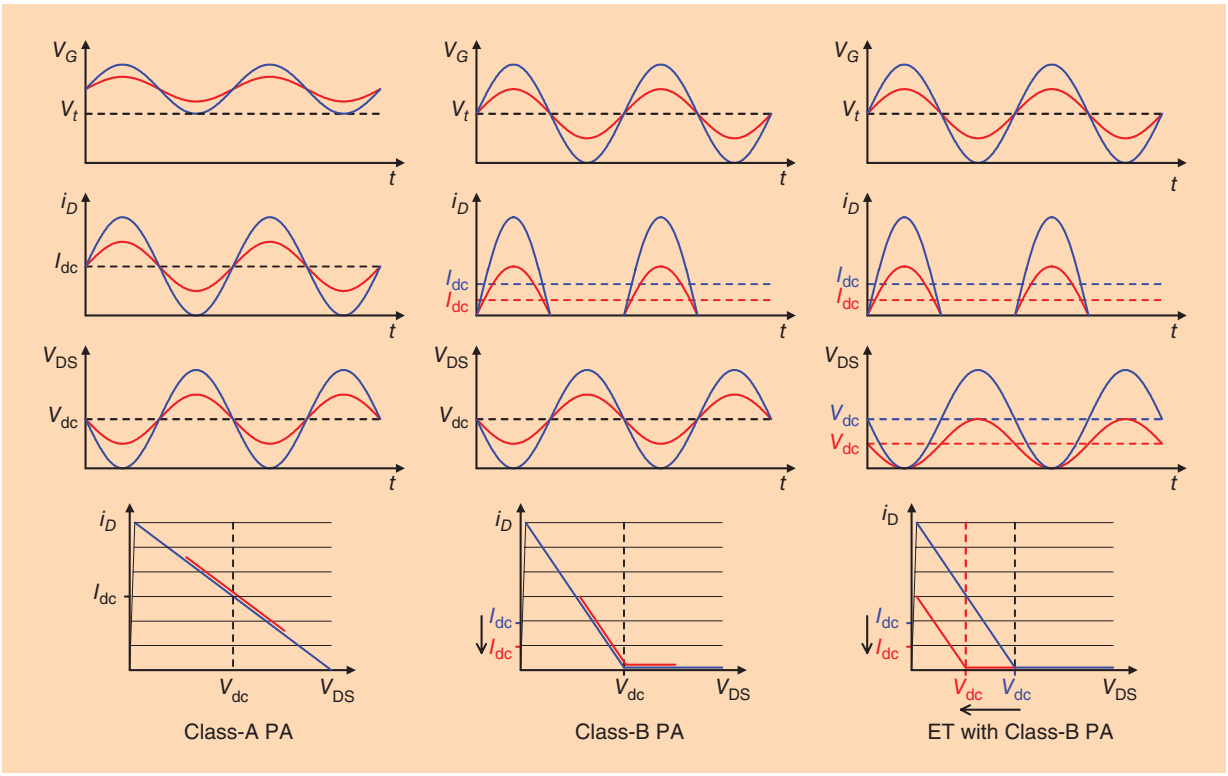

Figure 2. *Voltage and current waveforms and loadlines of class-A PA, class-B PA, and class-B ET PA.*

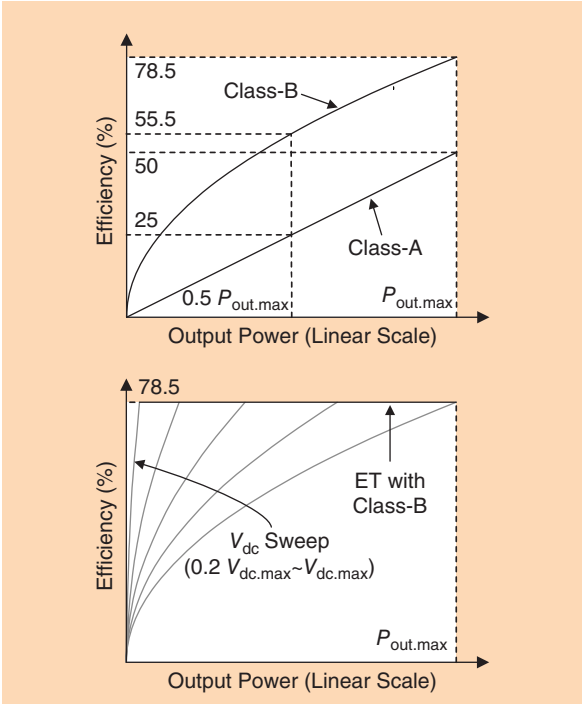

Figure 3. *Efficiency curves of class-A PA, class-B PA, and class-B ET PA for* $V_{knee} = 0$.

ear PA as in the conventional case for linear operation. Therefore, although the efficiency can be slightly lower than that in EER, all the other problems of the EER system are mitigated. Moreover, this ET structure is more suitable for amplification of wideband signals than the EER. Figure 2 shows the voltage and current waveforms and load lines of a class-A PA, class-B PA, and class-B ET PA. The black solid lines represent the case of maximum linear output power ($P_{out.max}$), and the gray solid lines represent the case with output power (P_{out}) that is one-quarter of $P_{out.max}$ (6 dB lower P_{out}). In this figure, zero knee voltage and uniform transconductance (g_m) are assumed to simplify calculation. When the class-A PA delivers 1/4 $P_{out.max}$, its dc power consumption does not change and its efficiency is significantly degraded by the fixed V_{dc} and I_{dc}. For the class-B PA, I_{dc} decreases as P_{out} decreases, but V_{dc} is fixed. Its efficiency decreases much slower than that of the class-A PA because of the decreased I_{dc}, which is proportional to the square root of P_{out}. For the class-B ET PA, V_{dc} is modulated by the supply modulator and I_{dc} is automatically controlled by the class-B bias. Therefore, its efficiency is constant for the entire output power range. Under the assumption of zero knee voltage and an ideal supply modulator,

$$\eta_A = 0.5\frac{P_{out}}{P_{out.max}}, \quad \eta_B = \frac{\pi}{4}\sqrt{\frac{P_{out}}{P_{out.max}}}, \quad \eta_{ET.B} = \frac{\pi}{4} \quad (1)$$

Figure 3 depicts the efficiencies of the three PAs according to P_{out} for ideal case of $V_{knee} = 0$. The class-B ET PA has efficiency of 78.5% for all output power range by tracking peak efficiency points of the class-B PA. When the knee voltage is one-tenth of the maximum V_{dc}, the efficiencies of the class-A and class-B PAs are

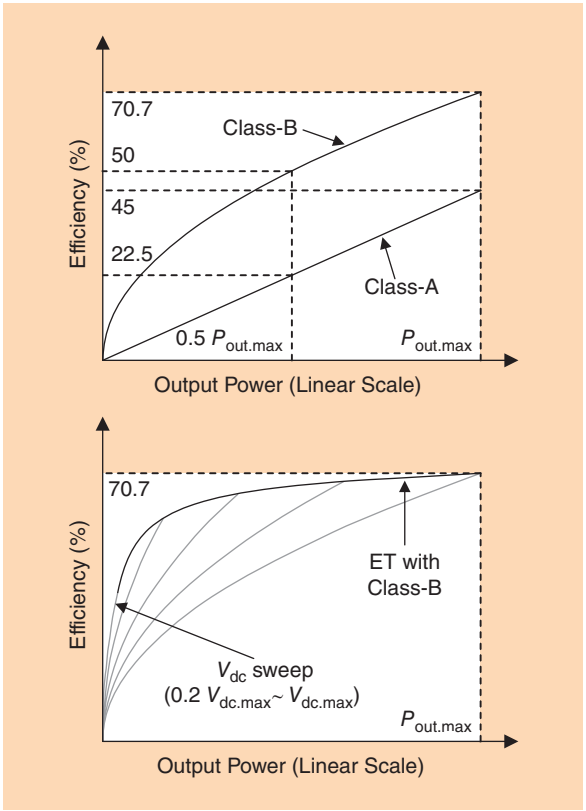

Figure 4. *Efficiency curves of class-A PA, class-B PA, and class-B ET PA for* $V_{knee} = 9/10\ V_{dc.max}$.

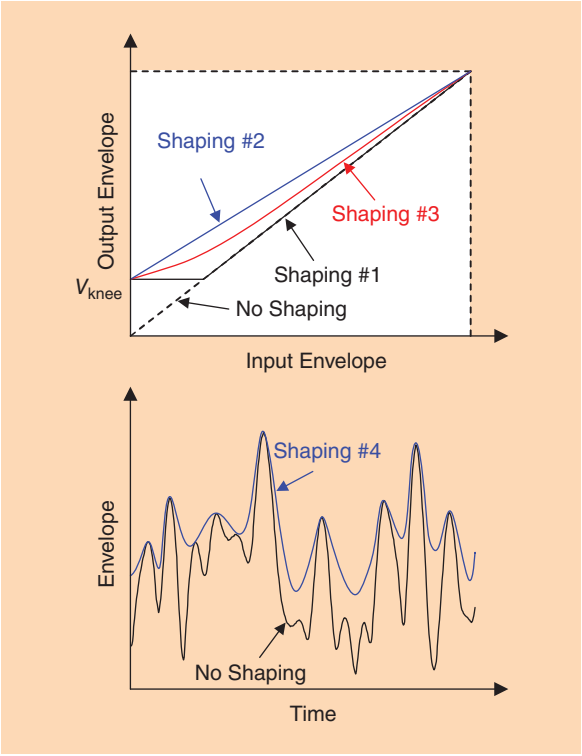

Figure 5. *Envelope shaping functions.*

nine-tenths of that in the case with zero knee voltage, and the efficiency of the ET PA decreases with P_{out} due to knee voltage, as shown in Figure 4.

Envelope Shaping

Generally, envelope shaping is an important technique to improve linearity, efficiency, and/or reduce the burden on the supply modulator. When the supply voltage to the PA is lower than the knee voltage, its nonlinear output capacitance increases suddenly, and the PA shows strong nonlinear characteristics by AM-AM and AM-PM distortions [16], [21]. To solve this problem, several envelope shaping functions have been proposed in [8], [9], [13], [14], and [18] in which the supply voltage is greater than the knee voltage. As shown in Figure 5, the shaping functions can be classified into five types (including the no-shaping case). Shaping function #1 clips the envelope to avoid voltages lower than the knee voltage. This abrupt curve expands the bandwidth of the envelope signal, but the AM-AM characteristic of the PA is not good. Shaping function #2 adds an offset voltage to the original envelope signal, and this operation does not change the bandwidth of the envelope signal. If the knee voltage is constant through the entire operating region, the offset voltage, which is equal to the knee voltage, removes the output voltage swing into the knee region. Shaping function #2 shows much better linearity and a slightly lower efficiency than shaping function #1. Shaping function #3 considers variations in the knee voltage and optimum efficiency. It shows intermediate characteristics between shaping functions #1 and #2. Shaping function #4 is different from the other functions: it reduces the bandwidth of the envelope signal for supply modulators with reduced bandwidth specifications [18]. Its disadvantage is lower efficiency and worse linearity than shaping functions #2 and #3. A summary of these envelope shaping functions is shown in Table 1.

Supply Modulator

For ET, the envelope signal from a modem or an envelope detector should be amplified and supplied to the drain of the PA. The supply modulator, which amplifies the envelope signal, should have a large bandwidth, larger than the envelope signal bandwidth, as well as high efficiency across this bandwidth. The bandwidth of the envelope signal is a few times wider than the bandwidth of the modulated signal, and it is not an easy task to amplify a wide-bandwidth signal with high efficiency. The hybrid switching amplifier (HSA) is the most popular supply modulator.

Structure of Supply Modulator

The HSA is a combination of a switching amplifier and a linear amplifier (Figure 6). In this architecture, the switching amplifier provides the required current as a slave amplifier, while the linear amplifier accurately

TABLE 1. Summary of envelope shaping functions.

	No Shaping	Shaping #1	Shaping #2	Shaping #3	Shaping #4
Efficiency	Very high	Very high	High	Very high	Good
Linearity	Bad	Not bad	Very good	Good	Normal
Envelope's BW	No change	Wider BW	No change	Wider BW	Reduced BW
Complexity	Very simple	Very simple	Very simple	Complex	Very complex

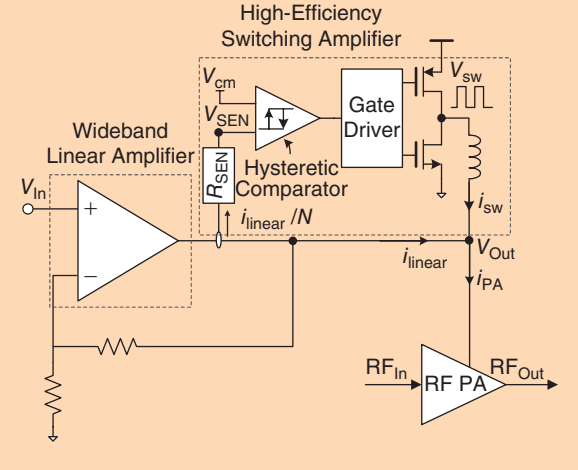

Figure 6. *Simplified architecture of the HSA supply modulator.*

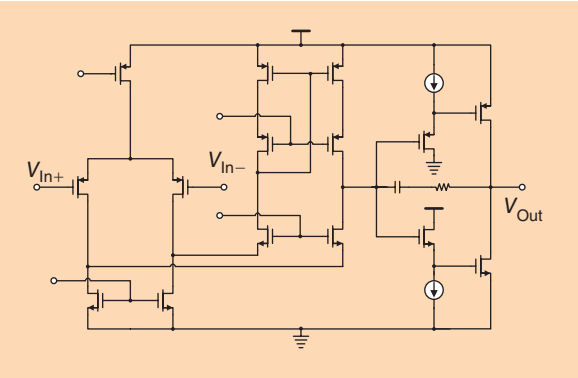

Figure 7. *Schematic of linear amplifier.*

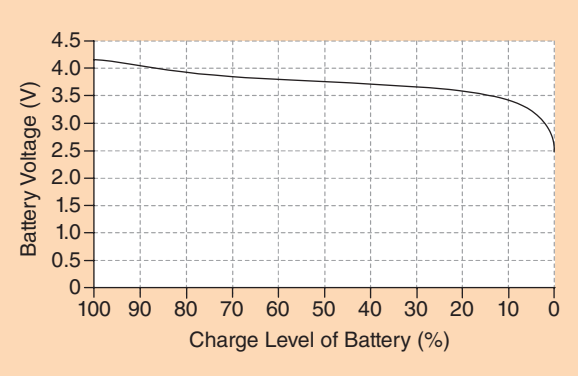

Figure 8. *Discharge curve of Li-Ion battery.*

generates the required voltage as a master amplifier and compensates for the ripple current of the switching amplifier. Usually, the switching amplifier supplies the low-frequency component of the envelope signal with high efficiency, and the linear amplifier provides the other high-frequency component with high speed. Since most of the power of the envelope signal is located at a low frequency, this architecture is suitable for wideband operation with high efficiency. The switcher is hysteretically controlled by the current flow from the linear amplifier. When the linear amplifier supplies a current, the switcher is turned on and vice versa.

The wideband linear amplifier operates as a voltage-controlled voltage source (VCVS). That is, the output voltage of the linear amplifier is the same as its input voltage owing to its high gain, wide bandwidth, and negative feedback loop. As shown in Figure 7, a folded-cascode operational transconductance amplifier (OTA) with a high gain is used as a linear amplifier to achieve a large bandwidth and high dc gain. For large-current-driving capabilities and rail-to-rail operation, the output buffer has a common-source configuration, and it is biased for class-AB operation, which affords linearity and efficiency.

The switching amplifier operates as a dependent current source. The direction of current flow through the linear amplifier is detected and used to control the switches using a hysteretic comparator. Generally, the average switching frequency is dependent on the hysteresis width, inductor value, and some other parameters for a narrowband signal. As introduced in [13], the switching frequency can be expressed as

$$f_{sw} = \frac{R_{sen} V_{out} (V_{dd} - V_{out})}{2 V_{dd} N L V_{hys}} \tag{2}$$

where V_{dd}, V_{hys}, R_{sen}, and N are the supply voltage, the hysteresis voltage of the comparator, the current-to-voltage ratio, and the current sensing ratio in the sensing unit, respectively.

For a wideband signal, the average switching frequency is mainly determined by its bandwidth. However, higher switching speeds reduce the efficiency. Thus, the switching speed should be optimized according to the signal bandwidth. As shown in (2), the switching speed can be easily controlled by adjusting the hysteretic value. The sizes of the power switches are determined by considering the conduction loss and switching loss at the specific load resistance, switching frequency, and duty ratio.

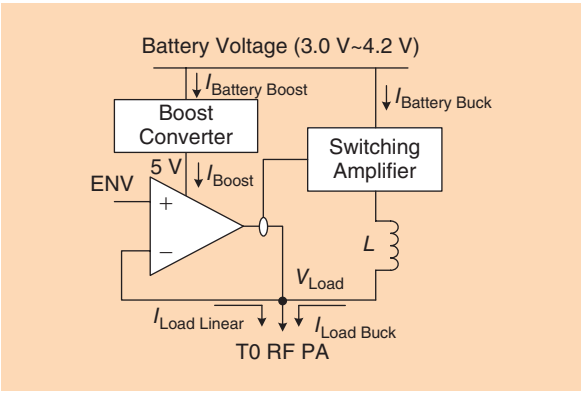

Figure 9. *Battery-to-5-V boosted PA supply modulator.*

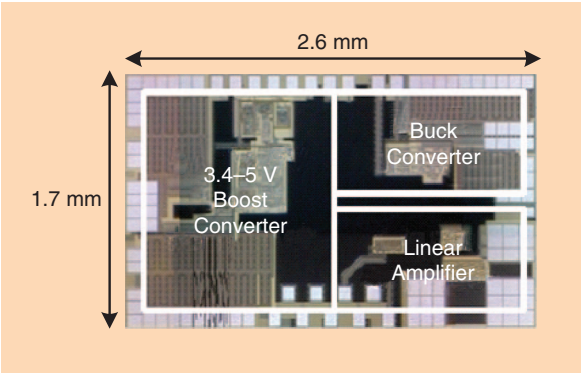

Figure 10. *Microphotograph of the fabricated boost-mode hybrid switching supply modulator.*

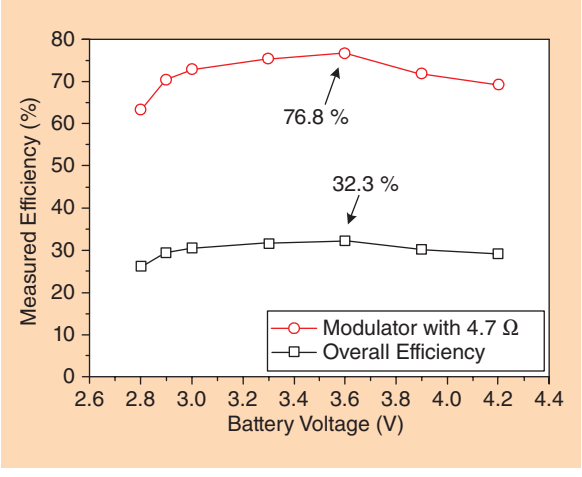

Figure 11. *Measured efficiencies of the 5-V-boosting envelope-tracking PA for LTE applications.*

Boost-Mode Supply Modulator

Figure 8 shows the output voltage characteristics of a lithium-ion (Li-ion) battery. When it is fully charged, the battery voltage is nearly 4.2 V, but as it discharges, the voltage drops gradually to below 3.2 V and drops very fast thereafter. Since the PA should transmit the required output power ($P_{out,min}$) under any circumstance, it should be designed for the worst case, i.e., a nominal battery level ($V_{DD,min}$) of 3.4 V. For a higher voltage, it will transmit more than the minimum required, thus

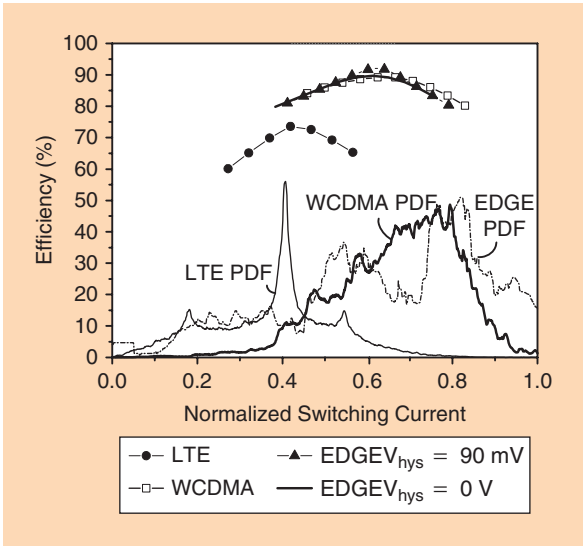

Figure 12. *Simulated average switching currents for LTE, WCDMA, and EDGE signals. The switching currents are normalized as 640 mA. The PDF of each signal is also depicted as a function of switching current (= $V_{out} = R_{load}$).*

wasting power. To simulate the practical operation environment of the ET PA, where the modulator is directly connected to a battery, a boost-mode hybrid switching supply modulator is introduced in [12]. As shown in Figure 9, the boost converter is only employed for the linear amplifier, while the buck converter is directly connected to the fluctuating battery. By boosting the supply voltage of the linear amplifier to a fixed 5 V regardless of the battery voltage variation, it provides a maximum supply voltage of 4.5 V to the PA, considering the 0.5-V drop across the modulator. The linear amplifier then operates with a boosted supply voltage and can regulate the load. The PA can be designed for operation at 4.5 V and can also realize good performance over the entire battery voltage range. The efficiency degradation due to the boost converter is minimal because a major part of power is generated by the switching amplifier, and the linear amplifier provides a small portion. The boosted voltage operation reduces the current level and directly results in a smaller die size and routing loss, which means lower cost and higher efficiency. Therefore, the boosted supply modulator may be an ideal power-management integrated circuit (PMIC) for a power amplifier.

The efficiency of the boost-mode supply modulator is expressed as follows:

$$\eta_{Boost} = \frac{5\,V \cdot I_{Boost}}{V_{Battery} \cdot I_{BatteryBoost}} \tag{3}$$

$$\eta_{Linear} = \frac{V_{Load} \cdot I_{LoadLinear}}{5\,V \cdot I_{Boost}} \tag{4}$$

$$\eta_{Buck} = \frac{V_{Load} \cdot I_{LoadBuck}}{V_{Battery} \cdot I_{BatteryBuck}} \tag{5}$$

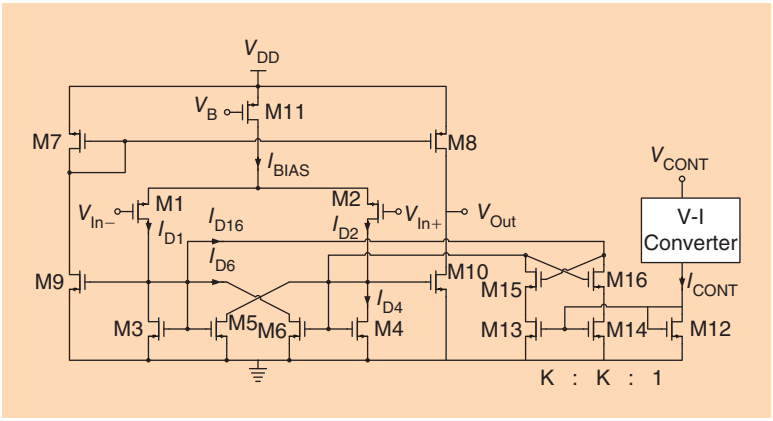

Figure 13. *Schematic of the programmable hysteretic comparator.*

TABLE 2. Performance summary of multimode supply modulator.

Parameters		Values
Supply voltage		3.3 V
Output voltage range		0.3–3 V
Output RMS current		0–750 mA
Peak efficiency		89%
Worst case GBW		120 MHz
f_{sw}	EDGE	2.12 MHz
	WCDMA	2.88 MHz
	m-WiMAX	3.75 MHz
V_{hys}	EDGE	20 mV
	WCDMA	0 mV
	m-WiMAX	0 mV

TABLE 3. Overall performance summary of ET PA.

Application	PAPR	BW	ηS.M	P_{out}	Gain	Overall PAE
EDGE	3.5 dB	384 kHz	84%	27.8 dBm	29.4 dB	45.3%
WCDMA	3.4 dB	3.84 MHz	84%	29 dBm	27.8 dB	46%
m-WiMAX	8.6 dB	5 MHz	75%	23.9 dBm	27.9 dB	34.3%

$$\eta_{\text{Overall}} = \frac{V_{\text{Load}} \cdot (I_{\text{LoadLinear}} + I_{\text{LoadBuck}})}{V_{\text{Battery}} \cdot (I_{\text{BatteryBoost}} + I_{\text{BatteryBuck}})} = (1-\alpha) \cdot \eta_{\text{Boost}} \cdot \eta_{\text{Linear}} + \alpha \cdot \eta_{\text{Buck}}, \quad (6)$$

where α is defined as the ratio of the dc current consumption from the buck converter ($I_{\text{BatteryBuck}}$) to the total dc current consumption from the battery ($I_{\text{BatteryBoost}} + I_{\text{BatteryBuck}}$). Figure 10 shows a die photograph for a 1-W supply modulator with a chip size of 2.6 mm × 1.7 mm including all pads.

The efficiency variation with the battery voltage is shown in Figure 11. There is no significant degradation in efficiency with changes in the battery voltage. The maximum efficiency of the modulator is 76.8% at 3.6 V. The implemented ET PA achieves the maximum efficiency of 32.3% with 25.8 dBm output power at a battery level of 3.6 V [12].

Multimode Supply Modulator

Multistandard signals have different PAPRs and bandwidths. Therefore, for MM operation, the transmitter should be adapted to the characteristics of each standard [13], [22]. Figure 12 shows the probability density function (PDF) and a plot of the efficiency of the supply modulator verses the switching current. The modulator should have an optimum efficiency at different switching currents for various envelope signals. As shown, the supply modulator can regulate the amount of current from the switcher according to the input signal's PAPR through the sensing and comparison mechanism so that the optimized efficiency profiles are achieved for different PAPR signals.

The switching frequency of the modulator is generally proportional to the signal bandwidth, and switching at higher frequencies generates higher switching loss. Therefore, the switching frequency should be optimized according to the signal bandwidth. However, the modulator design parameters are fixed for a certain application. For a modulator optimized for wideband signals, narrower-band signals will result in an excessively high switching frequency and high switching loss. Therefore, the modulator should be designed for a large-bandwidth signal, and the switching frequency should be lowered using variable hysteretic values for a narrower signal. To vary the switching frequency according to the input signal bandwidth, the programmable hysteresis operation is performed using the circuit shown in Figure 13 [13]. It consists of a conventional hysteretic comparator and a positive feedback control circuit. The additional feedback control circuit regulates the currents through M15 and M16. This has the effect of scaling the size of M5 and M6, which determine the amount of positive feedback. If it is assumed that the device sizes of M3, M4, M5, and M6 are the same, the effective positive feedback factor is given by

$$\alpha' = \frac{I_{\text{BIAS}} + K \cdot I_{\text{CONT}}}{I_{\text{BIAS}} - K \cdot I_{\text{CONT}}} \quad (7)$$

$$K = \frac{(W/L)_{13,14}}{(W/L)_{12}}. \quad (8)$$

The hysteresis voltage is expressed as

$$V_{\text{hyst}} \cong \sqrt{\frac{I_{\text{BIAS}}}{\mu_p C_{\text{ox}} (W/L)_{1,2}}} \cdot \frac{K \cdot I_{\text{CONT}}}{I_{\text{BIAS}}}. \quad (9)$$

With a linear voltage (V)–current (I) converter, V_{hyst} is linearly proportional to V_{CONT} with ±10 mV/V. Table 2 summarizes the performance of the MM supply modulator. The overall performance of the ET PA is also summarized in Table 3.

Envelope-Tracking Power Amplifier for Base Stations

Many studies have been conducted on ET PAs for base stations [23]–[25]. Since the ET PA is based on the interlock operation of a supply modulator and a PA, its two parts should be considered as an integrated whole for optimization of performance. However, previous studies have focused on the PA or supply modulator separately. In this section, we describe the fundamental operation of an ET PA for a base station and methods for improving the efficiency of the ET PA that are based on the interlock operation.

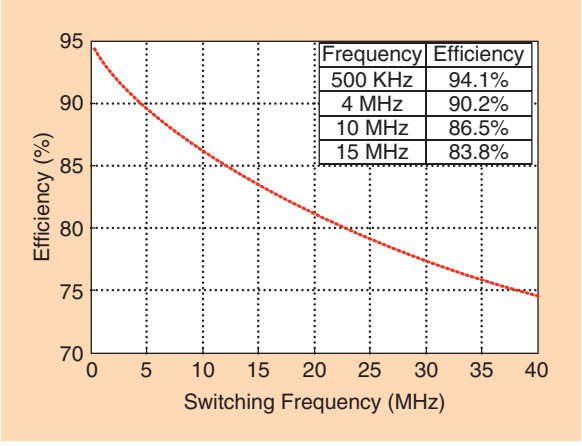

Figure 14. *Efficiency of the switching stage versus switching speed.*

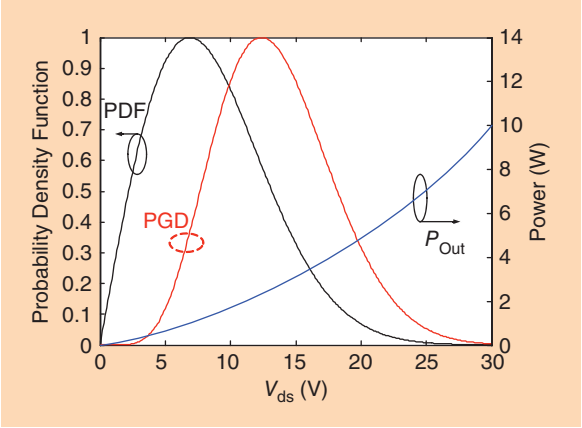

Figure 15. *PDF and PGD of the WCDMA signal with peak-to-average power ratio of 9.8 dB.*

Guideline for Optimization of ET PA

The HSA is the most popular supply modulator architecture; its fundamental operation was described in the previous section. The modulator is usually based on discrete components; however, some integrated modulators have been reported [26]. In advanced wireless communications, the envelope signal of the supply modulator must have a wide bandwidth and high PAPR to handle large volumes of multimedia data. To properly amplify the envelope signal with high efficiency, the switching stage supplies a quasi-constant current with high efficiency and the linear stage compensates for the error signal of the switcher by generating a sourcing current and a sinking current. The switching speed of the modulator follows the bandwidth of the envelope signal, and the efficiency of the switching stage decreases with an increase in the switching speed. Therefore, the overall efficiency of the modulator is also low for a large-bandwidth signal. Figure 14 shows the efficiency of the switcher versus the switching frequency. For the common operation of an HSA for a 20-MHz-bandwidth signal, the switching frequency is approximately 10 MHz and the efficiency is approximately 86%. To maintain high efficiency in the switching stage, the switching speed should be kept very low regardless of the bandwidth. The switching speed can be controlled by varying the hysteretic value of the hysteresis comparator. For a high hysteretic value, the switching speed can be reduced to several kilohertz with over 95% efficiency, and the overall efficiency of the modulator is also improved.

For ET, the PA is operated at a different drain bias voltage. Owing to the output capacitance variation, the PA cannot be matched across a large voltage range. Therefore, the efficiency of the PA should be optimized for the drain bias voltage at the highest power generation point. The average efficiency of the supply-modulated PA depends on the PDF of the complex-modulated input signal as follows:

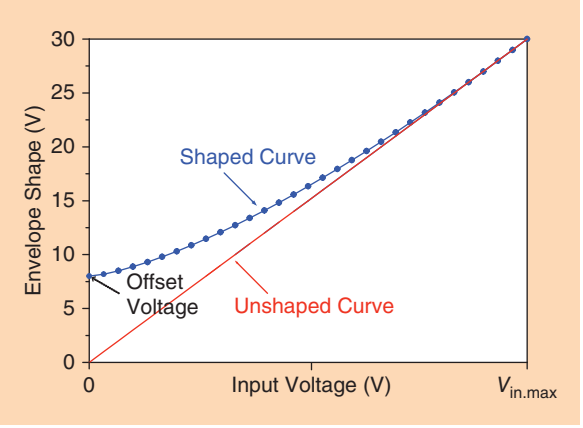

Figure 16. *Envelope shaping function for base station ET PA.*

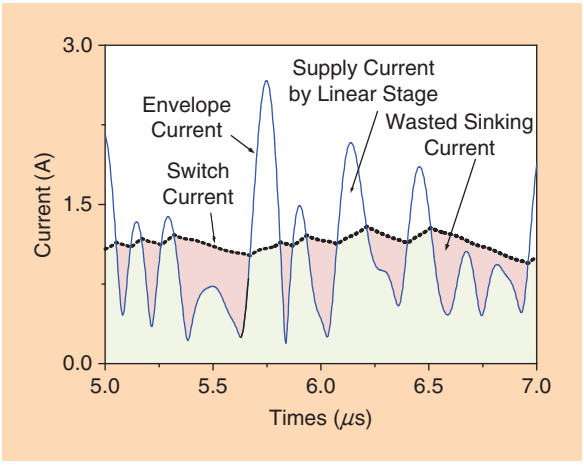

Figure 17. *Output current waveforms of a modulator.*

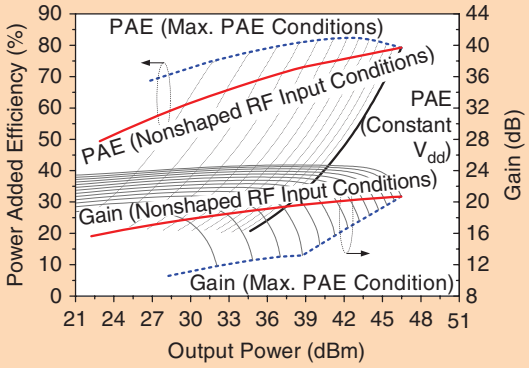

Figure 19. *PAE and gain characteristics of the ET PA for various drain biases.*

$$\eta_{\text{overall}} = \frac{\int \text{PDF}(V_{\text{DS}}) \cdot P_{\text{OUT}}(V_{\text{DS}}) dV_{\text{DS}}}{\int \text{PDF}(V_{\text{DS}}) \cdot P_{\text{DC}}(V_{\text{DS}}) dV_{\text{DS}}}. \quad (10)$$

In this equation, the power-generation distribution (PGD) is the product of the PDF and the output power. As shown in Figure 15, the point is significantly higher than the maximum PDF point because of the large power factor. Therefore, the PA should be designed for the highest efficiency at the maximum PGD point to obtain the highest efficiency overall [25].

Efficiency Enhancement Through Interlock Operation

For the ET PA, the envelope is the only element connecting the supply modulator and the PA. Because the envelope signal is the output waveform of the supply modulator and is also the drain bias of the PA, the envelope should be properly shaped to obtain the best performance from the ET PA. As we described in the previous session, we have found the shaping function that provides the best performance (Figure 16). The knee voltage of a GaN power transistor for base-station applications is approximately 5 V and the offset voltage should be greater than this. Thus, we can determine the minimum output envelope voltage above it and draw the shaping curve by softly following the linear envelope. When the offset voltage is larger, the efficiency of the supply modulator increases because the PAPR of the signal is reduced but the modulator supplies more than enough power for the PA. Thus, the efficiency of the PA is reduced. The detailed shape of the curve was decided by experiments since a simulator for the total ET system is not yet available.

The efficiency of the ET system can be enhanced by a proper interlock operation: we introduce two efficiency-improving techniques for base-station applications. The supply modulator is an ideal voltage source supplying the current required by the PA, which is determined by the RF input signal of the PA together with the gate dc bias. The switching stage in the supply modulator cannot supply a wideband envelope current and operates as a quasi-constant current source. The linear stage sources the insufficient current and sinks the

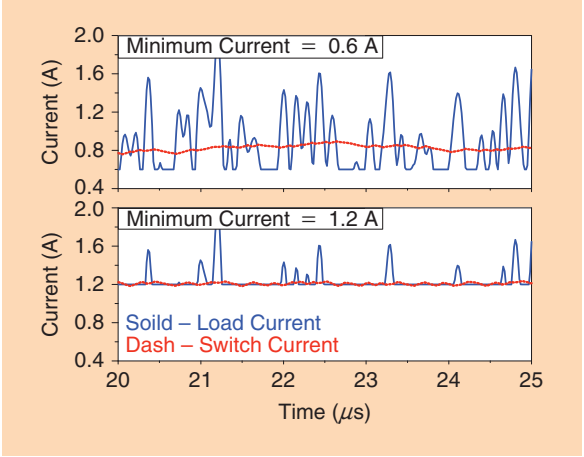

Figure 18. *Output current waveforms with different minimum load currents.*

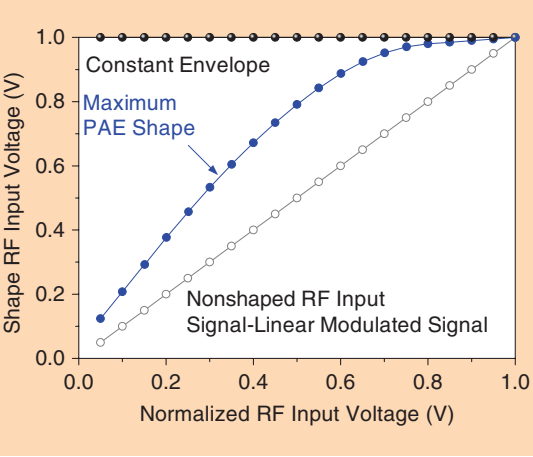

Figure 20. *RF input shaping functions.*

overflowed current, as shown in Figure 17. The overflowed current goes to the ground and is wasted. Instead of wasting the current, it can be redirected to the PA and utilized for amplification, which we call utilization of the sinking current (USC) [27]. For this purpose, the gate bias of the PA should be changed from deep class AB to class A. In this case, the quiescent bias current of the PA increases proportionally with the gate bias and the minimum load current of the modulator increases, reducing the sinking current. Figure 18 shows the load currents and switch currents versus the minimum load current required for the PA. When the minimum bias current of the PA is changed from 0.6 A to 1.2 A, most of the switch current flows to the load without any sinking current. Thus, the sinking current is delivered to the PA and utilized for RF amplification.

The other method for increasing the efficiency of the ET PA is RF input signal shaping (RFIS). ET PAs usually employ a modulated RF signal for the input to the PA. The modulated RF signal cannot saturate the PA uniformly over all power levels because of nonlinear and C_{gs} characteristics. Therefore, the PA cannot deliver maximum efficiency for all drain biases using the modulated RF input signal, as shown in Figure 19. To solve this problem, the RF input power should be increased at low power levels to push the device into high-PAE operation. Figure 20 shows the optimum input shaping curve to achieve the maximum PAE of the PA; this shaping can be implemented easily by a signal generator. This efficiency enhancement method is effective for a high-gain PA because the gain is compressed significantly.

An ET PA was implemented at 889 MHz by employing the USC and RFIS techniques and was tested using LTE signals with a bandwidth of 5 MHz and a PAPR of 6.5 dB. A saturated PA [28] was designed using a Cree CGH40045 GaN high-electron-mobility transistor (HEMT), with the optimized PAE at the maximum PGD point. The supply modulator was built using discrete components for the best performance. Table 4 shows a performance summary for the ET PAs. To utilize the wasted current for amplification of the signal in the PA, the gate bias was increased from −3.2 V to −2.5 V. The 2.5 V. The result is that the PAE was improved by 3.59%; the gain and output power were also improved. Additionally, the RFIS method was adopted for the interlock operation. As a result,

TABLE 4. ET PA performance at 889 MHz with the interlock techniques.

	PAE (%)	DE (%)	P_{out} (dBm)	Gain (dB)
Conventional	53.18	54.16	39.57	17.46
USC	56.77	57.63	40.00	18.26
RFIS	58.76	60.21	40.14	16.19

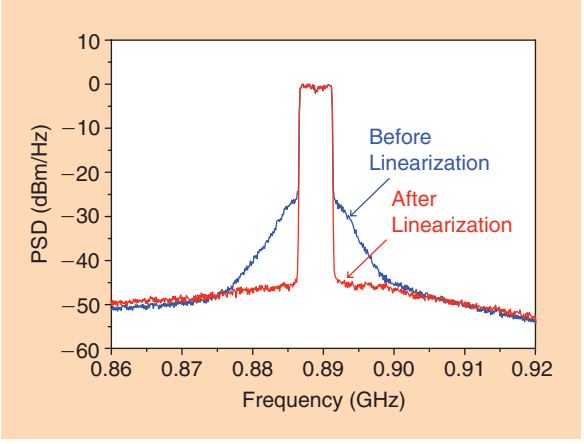

Figure 21. *Measured LTE spectra before and after DPD linearization.*

PAE improved by an additional 2% from the USC case. Thus, the proposed ET PA improved the PAE by 5.5% compared with the conventional case. Through linearization using the digital pre-distortion (DPD) techniques [29]–[30], the ET PA can be linearized properly to deliver an output power of 40.00 dBm with a PAE of 58.35%. The adjacent channel leakage ratios (ACLRs) at 7.5 MHz and 12.5 MHz offsets were reduced to below −45 dBc (Figure 21), which satisfies the linearity specification of the LTE system.

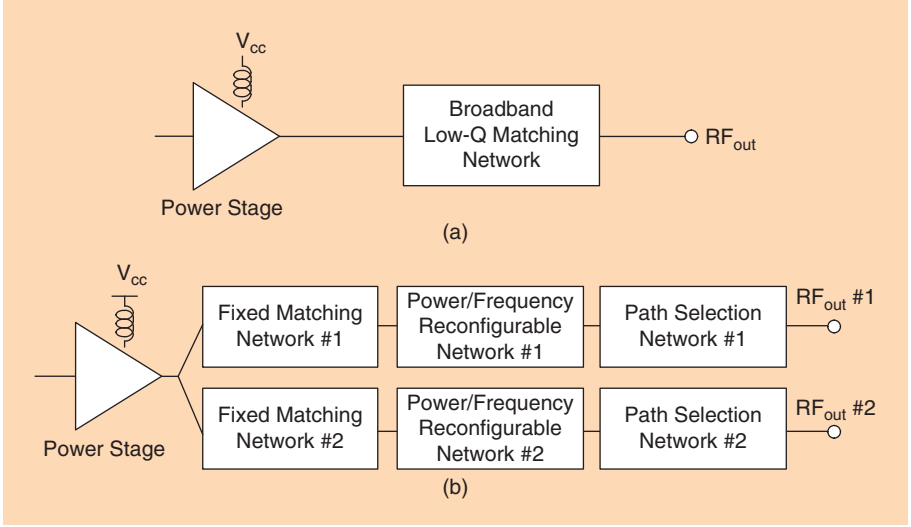

Figure 22. *(a) MB PA with broadband matching network. (b) MB PA with reconfigurable matching network.*

TABLE 5. LTE and UMTS (FDD) frequency allocations.

LTE and UMTS (FDD)			
Band	**Uplink Range (MHz)**	**Downlink Range (MHz)**	**Main Region(s)**
Band 1	1,920–1,980	2,110–2,170	Europe, Asia
Band 2	1,850–1,910	1,930–1,990	Americas (Asia)
Band 3	1,710–1,785	1,805–1,880	Europe, Asia (Americans)
Band 4	1,710–1,755	2,110–2,155	Americas
Band 5	824–849	869–894	Americas
Band 8	880–915	925–960	Europe, Asia

TABLE 6. LTE (TDD) frequency allocations.

LTE (TDD)		
Band	**Frequency Range (MHz)**	**Main Region(s)**
Band 33	1900–1920	Europe, Asia (not Japan)
Band 34	2010–2025	Europe, Asia
Band 35	1850–1910	Americas
Band 36	1930–1990	Americas

TABLE 7. GSM, DCS, and EDGE frequency allocations.

GSM, DCS, EDGE		
Band	**Frequency Range (MHz)**	**Main Region(s)**
GSM850	824–849	Europe, Americas
GSM900	880–915	Europe, Americas, Asia
DCS1800	1710–1785	Europe, Americas, Asia

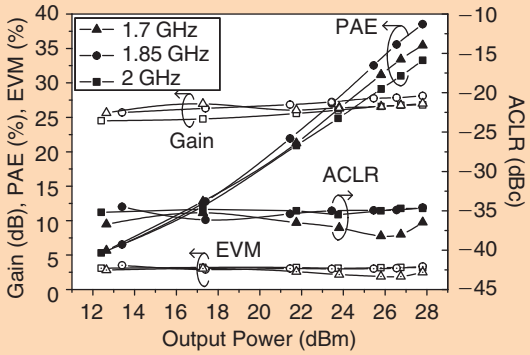

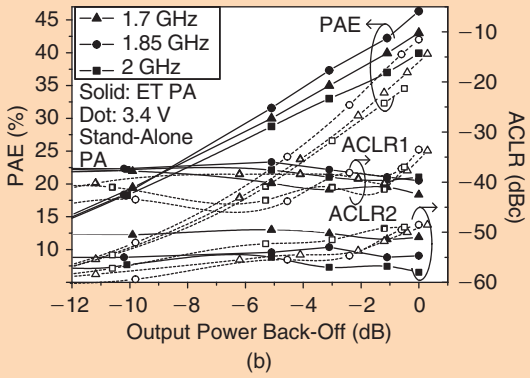

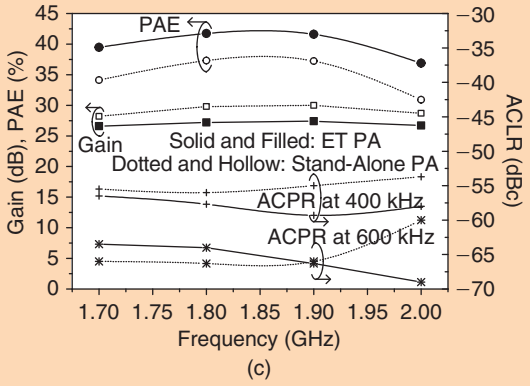

Figure 23. *(a) Measured performance of ET PA at 1.7–2 GHz for a 10-MHz-bandwidth 16-QAM 7.5-dB PAPR LTE signal. (b) Measured performance of ET PA and stand-alone PA for a 3.84-MHz-bandwidth 3.5-dB PAPR WCDMA signal at 1.7–2 GHz, and the maximum output powers are 30.1 and 28.1 dBm, respectively. (c) Measured performance of ET PA and stand-alone PA for EDGE signals at output powers of 28 and 27 dBm, respectively, at 1.7–2 GHz.*

Envelope-Tracking Power Amplifier for Handsets

MM/MB PAs enable worldwide global roaming for mobile handsets, which has become an important issue. PAs based on GaAs heterojunction bipolar transistors (HBTs) show good performance not only in terms of efficiency but also linearity owing to their high breakdown voltage and low knee voltage characteristics. Many studies on ET PAs for handsets have been carried out using such HBTs. The supply modulator for ET is generally implemented at a CMOS foundry. Therefore, the GaAs HBT PA is in conjunction with a CMOS supply modulator on the PCB, composing a hybrid structure. Recently, many researchers have turned their attention to the development of CMOS-based linear PAs, which can be co-integrated with the supply modulator on the same die for a one-chip solution.

The boosted supply modulator structure, which was explained in the "Boost-Mode Supply Modulator" section, has many advantages for use in a PMIC. The ET PA has a major advantage for MM/MB operation since MM and MB can be handled separately; that is, the MM operation is provided through the MM

supply modulator [12], [22] as described in the "Multimode Supply Modulator" section, whereas the MB operation is handled separately by the PA without considering the MM operation. These concepts are addressed in the next section with the ET operation. For enhanced efficiency in a back-off region, the use of a PA with a tunable load is the most popular approach when using a handset PA without a supply modulator. A PA with a tunable load can be combined with a supply modulator to achieve great improvement in efficiency over the entire back-off power region.

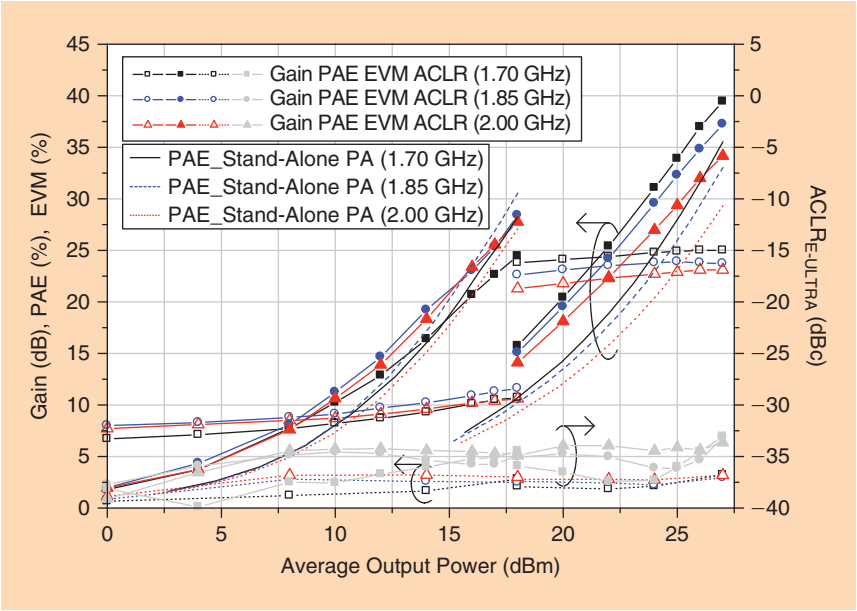

Figure 25. *Measured performance of the dual-power-mode ET PA with 16-QAM 7.5-dB PAPR LTE signal across the average output power.*

Multimode Multiband Power Amplifier with Envelope Tracking

Tables 5–7 show the LTE, UMTS (WCDMA), GSM, and EDGE frequency allocations. As you can see in the tables, the signals are intensively distributed over both a high-frequency band (1.7–2.0 GHz) and a low-frequency band (820–915 MHz). For the MM/MB operation in the ET system, the PA should cover the high- and low-frequency bands and the supply modulator should properly handle the MM signals [13]. There are two types of MB PAs. One is the broadband-matched PA using a low-Q network, as shown in Figure 22(a). The output matching network comprises a broadband fundamental impedance matching circuit, second-harmonic tune circuits, and a third-harmonic tune circuit to maximize the efficiency [22]. PAs with this structure can deliver good efficiency and linearity at high or low frequency. Owing to the low-Q matching, the efficiency is slightly degraded as compared with a high-Q matching network targeted for only one band. A PA with a reconfigurable matching network is another alternative for MB operation, which can minimize the efficiency degradation using multiple paths that are optimized for each band, as shown in Figure 22(b) [31]. The reconfigurable matching network must include two or more switches for path selection, and the multiple paths require many passive components. Therefore, the structure is complex, which increases the circuit losses. For ET, the simple structure of an MB PA with a broadband matching network is preferred. Multistandard signals have different PAPRs and bandwidths that the modulator should handle properly. As described in the "Multimode Supply Modulator" section, the switching currents are automatically adapted to various PAPRs by the current sensing circuit and the hysteretic comparator in the HSA. Since the efficiency of the modulator decreases with an increase in the switching speed, the switching speed should be low but still sufficiently high to handle the signal. For an MM HSA design, the switching condition is optimized for the wideband signal by determining the required inductor value at the output of the switching stage. For a narrowband signal whose slew rate is lower than that of the switching amplifier, this HSA leads to an excessively high switching frequency and poor efficiency of the switching stage. Thus, we utilize a programmable hysteretic comparator, which enables us to control the hysteresis voltage and the switching frequency. The efficiency of the HSA is enhanced by approximately 3% through controlling

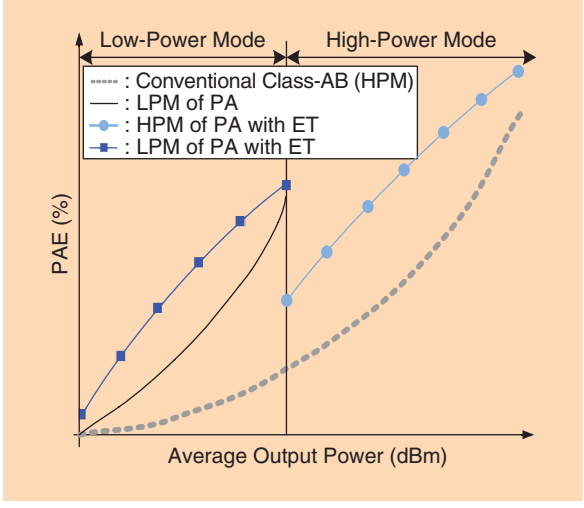

Figure 24. *PAE curves of the dual mode with ET PA.*

TABLE 8. Comparison table.

	Technology	Frequency	Application	PAPR/BW	P_{OUT}	PAE	ACLR(ACPR)
[35]	HBT GaAs	2.535 GHz	LTE	6.6 dB/20 MHz	29*	43%*	$ACLR1_{UTRA}$[1]: −49 dBc*
[36]	0.18-μm CMOS	1.85 GHz	WCDMA	3.5 dB/3.84 MHz	27.8	45.8%	$ACLR1_{UTRA}$[2]: −33 dBc
MMMB ET PA [22]	HBT GaAs	1.7–2.0 GHz	LTE	7.5 dB/10 MHz	28 dBm	33%–39%	$ACLR_{E\text{-}UTRA}$[1]: −35 dBc
			WCDMA	3.5 dB/3.84 MHz	30.1 dBm	40%–46%	$ACLR1_{UTRA}$[2]: −35 dBc
			EDGE	3.5 dB/384 KHz	28 dBm	37%–42%	ACPR[3] : −63 dBc (@600 kHz)
Dual Power Mode ET PA [32]	HBT GaAs	1.7–2.0 GHz	LTE	7.5 dB/10 MHz	10 dBm	10.2%–11.3%	$ACLR_{E\text{-}UTRA}$[1]: −34.5 dBc
					18 dBm	24.5%–28.4%	$ACLR_{E\text{-}UTRA}$[1]: −34.5 dBc
					27 dBm	34.2%–39.5%	$ACLR_{E\text{-}UTRA}$[1]: −33.1 dBc
CMOS ET PA [34]	0.18-μm CMOS	1.85 GHz	LTE	7.5 dB/10 MHz	26 dBm	33.5%	$ACLR_{E\text{-}UTRA}$[1]: −32.5 dBc

[1]LTE specifications: $ACLR_{E\text{-}UTRA} < -30$ dBc, $ACLR1_{UTRA} < -33$ dBc
[2]WCDMA specification: $ACLR1_{UTRA} < -33$dBc
[3]EDGC specification: ACPR < −60dBc
*with DPD

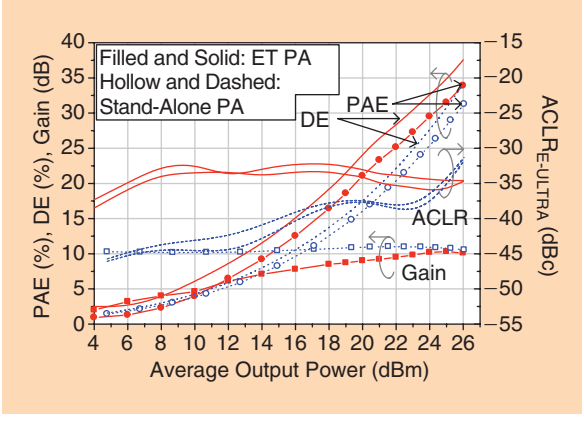

Figure 26. *Measured performance of the CMOS ET PA with 16-QAM 7.5-dB PAPR LTE signals.*

the hysteresis voltage of the EDGE signal. Figure 23 shows the measurement results for an MM/MB ET PA. The graphs show that the measured results satisfy the specifications for each signal standard with good performance [22].

Back-Off Efficiency Enhanced ET PA

To enhance efficiency in a back-off power region, the use of a PA with a tunable load is the most popular approach in handset applications. A boosted supply modulator can be implemented to further improve the efficiency in all power ranges. Figure 24 shows the conceptual curve of the PAE for a dual power-mode ET PA. In a recently reported paper, it was shown that a dual-mode PA can be operated as an MB PA and can realize good performance at high frequencies of 1.7–2.0 GHz [32]; the performance graph is shown in Figure 25. This structure is promising for handset PA applications.

CMOS ET PA

The conversional ET PA based on GaAs HBTs has a hybrid structure. However, by utilizing a CMOS-based linear PA, the CMOS supply modulator can be co-integrated on the same die, thus reducing the size and cost of the handset PA. However, it is not an easy task to replace the conventional GaAs HBT PA with a CMOS PA. CMOS has several defects compared with GaAs HBTs. The three major problems are the low breakdown voltage, lack of support of ground vias, and high substrate loss. Many research efforts have been devoted to overcoming these problems, and recently, highly linear CMOS PAs have started to appear in the market. Recent papers on CMOS PAs [33] and ET PAs [34] show that a highly linear PA can be achieved by using CMOS. The performance parameters of the devices reported in these papers are compared in Figure 26. With advanced design techniques, further performance improvements may be possible by replacing the GaAs HBT PAs.

Summary

The ET technique is designed to efficiently amplify a modulated signal with high PAPR through drain-bias modulation. The drain bias follows a shaped envelope of the modulated signal. For this purpose, we need a highly efficient supply modulator with a wide bandwidth. The ET PA achieves high efficiency for amplification of a signal with a large PAPR. Moreover, it is quite flexible for MM and MB operations. The supply modulator itself is an ideal PMIC for PAs. Therefore, the ET technique is quite a powerful tool for both base-station PAs and handset PAs. As the technique develops further, it will be widely employed in PAs for next-generation systems.

References

[1] L. Kahn, "Single-sideband transmission by envelope elimination and restoration," *Proc. IRE*, vol. 40, no. 7, pp. 803–806, Jul. 1952.

[2] P. Reynaert and M. S. J. Steyaert, "A 1.75-GHz polar modulated CMOS RF power amplifier for GSM-EDGE," *IEEE J. Solid-State Circuits*, vol. 40, no. 12, pp. 2598–2608, Dec. 2005.

[3] J. S. Walling, S. S. Taylor, and D. J. Allstot, "A class-G supply modulator and class-E PA in 130 nm CMOS," *IEEE J. Solid-State Circuits*, vol. 44, no. 9, pp. 2339–2347, Sept. 2009.

[4] G. Hanington, P. Chen, P. M. Asbeck, and L. E. Larson, "High-efficiency power amplifier using dynamic power-supply voltage for CDMA applications," *IEEE Trans. Microwave Theory Tech.*, vol. 47, no. 8, pp. 1471–1476, Aug. 1999.

[5] B. Sahu and G. A. Rincón-Mora, "A high-efficiency linear RF power amplifier with a power-tracking dynamically adaptive buck-boost supply," *IEEE Trans. Microwave Theory Tech.*, vol. 52, no. 1, pp. 112–120, Jan. 2004.

[6] V. Pinon, F. Hasbani, A. Giry, D. Pache, and C. Garnier, "A single-chip WCDMA envelope reconstruction LDMOS PA with 130 MHz switched-mode power supply," in *IEEE Int. Solid-State Circuits Conf. Tech. Dig.*, Feb. 2008, pp. 564–565.

[7] J. Kitchen, W. Chu, I. Deligoz, S. Kiaei, and B. Bakkaloglu, "Combined linear and Δ -modulated switched-mode PA supply modulator for polar transmitters," in *IEEE Int. Solid-State Circuits Conf. Tech. Dig.*, Feb. 2007, pp. 82–83.

[8] F. Wang, A. H. Yang, D. F. Kimball, L. E. Larson, and P. M. Asbeck, "Design of wide-bandwidth envelope-tracking power amplifiers for OFDM applications," *IEEE Trans. Microwave Theory Tech.*, vol. 53, no. 4, pp. 1244–1255, Apr. 2005.

[9] M. Hassan, L. E. Larson, V. W. Leung, D. F. Kimball, and P. M. Asbeck, "A wideband CMOS/GaAs HBT envelope tracking power amplifier for 4G LTE mobile terminal applications," *IEEE Trans. Microwave Theory Tech.*, vol. 60, no. 5, pp. 1321–1330, May 2012.

[10] T. Kwak, M. Lee, and G. Cho, "A 2 W CMOS hybrid switching amplitude modulator for EDGE polar transmitters," *IEEE J. Solid-State Circuits*, vol. 42, no. 12, pp. 2666–2676, Dec. 2007.

[11] W. Chu, B. Bakkaloglu, and S. Kiaei, "A 10-MHz-bandwidth 2-mV-ripple PA-supply regulator for CDMA transmitters," in *IEEE Int. Solid-State Circuits Conf. Tech. Dig.*, Feb. 2008, pp. 448–449.

[12] J. Choi, D. Kim, D. Kang, and B. Kim, "A new power management IC architecture for envelope tracking power amplifier," *IEEE Trans. Microwave Theory Tech.*, vol. 59, no. 7, pp. 1796–1802, July 2011.

[13] J. Choi, D. Kim, D. Kang, and B. Kim, "A polar transmitter with CMOS programmable hysteretic-controlled hybrid switching supply modulator for multistandard applications," *IEEE Trans. Microwave Theory Tech.*, vol. 57, no. 7, pp. 1675–1686, July 2009.

[14] D. Kim, D. Kang, J. Choi, J. Kim, Y. Cho, and B. Kim, "Optimization for envelope shaped operation of envelope tracking power amplifier," *IEEE Trans. Microwave Theory Tech.*, vol. 59, no. 7, pp. 1787–1795, July 2011.

[15] I. Kim, J. Kim, J. Moon, and B. Kim, "Optimized envelope shaping for hybrid EER transmitter of mobile WiMAX," *IEEE Microwave Wireless Compon. Lett.*, vol. 19, no. 5, pp. 335–337, May 2009.

[16] J. Moon, J. Son, J. Lee, and B. Kim, "A multimode/multiband envelope tracking transmitter with broadband saturated amplifier," *IEEE Trans. Microwave Theory Tech.*, vol. 59, no. 12, pp. 3463–3473, Dec. 2011.

[17] J. Hoversten and Z. Popovic, "Envelope tracking transmitter system analysis method," in *Proc. IEEE Radio Wireless Symp.*, New Orleans, LA, Jan. 2010, pp. 180–183.

[18] J. Jeong, D. F. Kimball, M. Kwak, C. Hsia, P. Draxler, and P. M. Asbeck, "Wideband envelope tracking power amplifier with reduced bandwidth power supply waveform," in *IEEE MTT-S Int. Microwave Symp. Dig.*, Boston, MA, June 2009, pp. 1381–1384.

[19] J. Jeong, D. F. Kimball, M. Kwak, P. Draxler, and P. M. Asbeck, "Envelope tracking power amplifiers with reduced peak-to-average power ratio RF input signals," in *Proc. IEEE Radio Wireless Symp.*, New Orleans, LA, Jan. 2010, pp. 112–115.

[20] F. H. Raab, "Intermodulation distortion in Kahn-technique transmitters," *IEEE Trans. Microwave Theory Tech.*, vol. 44, no. 12, pp. 2273–2278, Dec. 1996.

[21] J. C. Pedro, J. A. Garcia, and P. M. Cabral, "Nonlinear distortion analysis of polar transmitters," *IEEE Trans. Microwave Theory Tech.*, vol. 55, no. 12, pp. 2757–2765, Dec. 2007.

[22] D. Kang, D. Kim, J. Choi, J. Kim, Y. Cho, and B. Kim, "A multimode/multiband power amplifier with a boosted supply modulator," *IEEE Trans. Microwave Theory Tech.*, vol. 58, no. 10, pp. 2598–2608, Oct. 2010.

[23] D. F. Kimball, J. Jeong, C. Hsia, P. Draxler, S. Lanfranco, W. Nagy, K. Linthicum, L. E. Larson, and P. M. Asbeck, "High-efficiency envelope tracking W-CDMA base station amplifier using GaN HFETs," *IEEE Trans. Microwave Theory Tech.*, vol. 54, no. 11, pp. 3848–3856, Nov. 2006.

[24] F. Wang, D. Kimball, J. Popp, A. Yang, D. Lie, P. Asbeck, and L. Larson, "An improved power-added efficiency 19-dBm hybrid envelope elimination and restoration power amplifier for 802.11g WLAN applications," *IEEE Trans. Microwave Theory Tech.*, vol. 54, no. 12, pp. 4086–4099, Dec. 2006.

[25] I. Kim, Y. Woo, J. Moon, J. Kim, J. Moon, J. Kim, and B. Kim, "High efficiency hybrid EER transmitter using optimized power amplifier," *IEEE Trans. Microwave Theory Tech.*, vol. 56, no. 11, pp. 2582–2593, Nov. 2008.

[26] C. Hsia, A. Zhu, J. Yan, P. Draxler, D. Kimball, S. Lanfranco, and P. Asbeck, "Digitally assisted dual-switch high-efficiency envelope amplifier for envelope-tracking base-station power amplifiers," *IEEE Trans. Microwave Theory Tech.*, vol. 59, no. 11, pp. 2943–2952, Nov. 2011.

[27] J. Kim, J. Moon, J. Son, S. Jee, J. Lee, J. Cha, I. Kim, and B. Kim, "Highly efficient envelope tracking transmitter by utilizing sinking current," in *Proc. 41th IEEE European Microwave Conf.*, Manchester, U.K., Oct. 2011, pp. 636–639.

[28] J. Kim, J. Kim, J. Moon, J. Son, I. Kim, S. Jee, and B. Kim, "Saturated power amplifier optimized for efficiency using self-generated harmonic current and voltage," *IEEE Trans. Microwave Theory Tech.*, vol. 59, no. 8, pp. 2049–2058, Aug. 2011.

[29] Y. Y. Woo, J. Kim, J. Yi, S. Hong, I. Kim, J. Moon, and B. Kim, "Adaptive digital feedback predistortion technique for linearizing power amplifiers," *IEEE Trans. Microwave Theory Tech.*, vol. 55, no. 5, pp. 932–940, May 2007.

[30] J. Kim, Y. Y. Woo, J. Moon, and B. Kim, "A new wideband adaptive digital predistortion technique employing feedback linearization," *IEEE Trans. Microwave Theory Tech.*, vol. 56, no. 2, pp. 385–392, Feb. 2008.

[31] U. Kim, S. Kang, J. Woo, Y. Kwon, and J. Kim, "A multi-band reconfigurable power amplifier for UMTS handset applications," in *Proc. IEEE Radio Frequency Integrated Circuits Symp.*, Anaheim, CA, 2010, pp. 175–178.

[32] Y. Cho, D. Kang, J. Kim, D. Kim, B. Park, and B. Kim, "A dual power-mode multi-band power amplifier with envelope tracking for handset application," submitted for publication.

[33] B. Park, D. Kang, D. Kim, Y. Cho, C. Zhao, J. Kim, Y. Na, and B. Kim, "A 31.5%, 26 dBm LTE CMOS power amplifier with harmonic control," submitted for publication.

[34] D. Kang, B. Park, D. Kim, J. Kim, Y. Cho, and B. Kim, "Envelope-tracking CMOS power amplifier module for LTE applications," submitted for publication.

[35] M. Hassan, L. E. Larson, V. W. Leung, D. F. Kimball, and P. M. Asbeck, "A wideband CMOS/GaAs HBT envelope tracking power amplifier for 4G LTE mobile terminal applications," *IEEE Trans. Microwave Theory Tech.*, vol. 60, no. 5, pp. 1321–1330, May 2012.

[36] B. Koo, Y. Na, and S. Hong, "Integrated bias circuits of RF CMOS cascode power amplifier for linearity enhancement," *IEEE Trans. Microwave Theory Tech.*, vol. 60, no. 2, pp. 340–351, Feb. 2012.